



Convective environment in pre-monsoon and monsoon conditions over the Indian subcontinent: the impact of surface forcing

Lois Thomas¹, Neelam Malap¹, Wojciech W. Grabowski^{2,3}, Kundan Dani¹, and Thara V. Prabha¹

¹Indian Institute of Tropical Meteorology, Pune, India

²National Center for Atmospheric Research, Boulder, Colorado, USA

³Institute of Geophysics, Faculty of Physics, University of Warsaw, Warsaw, Poland

Correspondence to: Thara V. Prabha (thara@tropmet.res.in)

1 **Abstract.** Thermodynamic soundings for premonsoon and monsoon seasons from the Indian subcontinent are analyzed to
2 document differences between convective environments. Pre-monsoon environment features more variability for both near-
3 surface moisture and free-tropospheric temperature and moisture profiles. As a result, level of neutral buoyancy (LNB) and
4 pseudo-adiabatic Convective Available Potential Energy (CAPE) vary more for the pre-monsoon environment. Pre-monsoon
5 soundings also feature higher Lifting Condensation Levels (LCLs). LCL heights are shown to depend on the availability of
6 surface moisture, with low LCLs corresponding to high surface humidity arguably because of the availability of soil moisture. A
7 simple theoretical argument is developed and showed to mimic the observed relationship between LCL and surface moisture.
8 We argue that the key element is the partitioning of surface energy flux into its sensible and latent components, that is, the
9 surface Bowen ratio, and the way Bowen ratio affects surface buoyancy flux. We support our argument with observations of
10 changes in the Bowen ratio and LCL height around the monsoon onset, and with idealized simulations of cloud fields driven
11 by surface heat fluxes with different Bowen ratios.

12 1 Introduction

13 Convective environment over the Indian subcontinent changes significantly from hot and dry pre-monsoon conditions to cooler
14 and wetter monsoon. The change comes from the dramatic evolution of the large-scale circulation (e.g., Yin, 1949; Lau and
15 Yang, 1996 and references therein) that brings significant oceanic moisture during the monsoon. The conveyor belt of mois-
16 ture is the monsoon low-level jet (Joseph and Sijikumar, 2004) that moistens land areas, changes cloud characteristics, and
17 brings monsoon rains that are key to the Indian economy. The change from pre-monsoon to monsoon conditions is rapid with
18 convective precipitation driven by the surface heating in the pre-monsoon period giving way to an increase in cloud cover and
19 surface rainfall during the monsoon season (e.g., Ananthakrishnan and Soman, 1988). Significant rainfall occurs over the west
20 coast and the northeastern region, and it further extends westward in association with the northwestward movement of weather
21 systems formed over the Bay of Bengal (Gadgil et al., 1984).

22 The monsoon low-level jet weakens during the monsoon break periods, influencing moisture content over land and strongly
23 reducing the rainfall (Sandeep et al., 2014; Balaji et al., 2017). Intraseasonal oscillations of monsoon rainfall are well docu-
24 mented (e.g., Goswami and Mohan, 2001; Gadgil, 2003) with active and break periods featuring considerable spatiotemporal



25 variations (Rajeevan et al., 2010). Initial studies of the monsoon boundary layers focused on the contrast between active and
26 break monsoon periods (e.g.,Parasnis et al., 1985) with a contrasting moisture availability in the lower troposphere. The ac-
27 tive/break monsoon conditions are characterized by lower/higher boundary layer heights (e.g., Kusuma et al., 1991). Higher
28 cloud bases also occur during weak monsoon conditions when lower atmosphere is drier compared to the active monsoon.
29 Parasnis and Goyal (1990) reports enhanced convective instability in the boundary layer on weak monsoon days when com-
30 pared to the active monsoon. Convective Available Potential Energy (CAPE), a proxy for the strength of convection, feature
31 higher values over coastal regions because of the presence of higher moisture in the boundary layer (Alappattu and Kun-
32 hikrishnan, 2009). That study argues that the temporal variability of CAPE and convective inhibition (CIN) is predominantly
33 controlled by the boundary-layer moisture. Resmi et al. (2016) shows that sustaining convective storms in the diurnal cycle
34 is possible because of moisture advection and increase of CAPE over rain shadow region of the Indian subcontinent. Diurnal
35 variations of CAPE are directly linked to water vapor content near surface, with higher CAPE environments favoring higher
36 precipitation (Balaji et al., 2017). Precipitable water (PW) and lifting condensation level (LCL) derived from various obser-
37 vations are also closely related (Murugavel et al., 2016). Balaji et al. (2017) shows that high PW conditions correspond to
38 shallower boundary layer (with boundary layer height close to LCL) and higher LCL combined with deeper boundary layer
39 height typically occur during drier conditions. Balaji et al. (2017) also illustrates diurnal variations of PW and CAPE during
40 wet and dry regimes within the monsoon.

41 The monsoon onset marks a striking change in the surface and boundary layer conditions because of the change of the parti-
42 tioning of the surface energy flux into its sensible and latent components. However, there are no comprehensive comparisons of
43 pre-monsoon and monsoon thermodynamic environments and their contrasting characteristics with respect to parcel buoyancy
44 and boundary layer characteristics. The soil moisture variations typically follow rainfall patterns or variations. Transition from
45 pre-monsoon to monsoon conditions is associated with increase in soil moisture (Sathyanadh et al., 2016) and thus with the
46 change of the partitioning of the surface energy flux into its sensible and latent fluxes. The ratio of the sensible to latent surface
47 heat fluxes is commonly referred to as Bowen ratio. Bowen ratio affects surface buoyancy flux that drives boundary layer dy-
48 namics (e.g., Stevens, 2007 and references therein) and affects the rate at which convective boundary layer deepens. It also sets
49 the mean boundary layer humidity (e.g., Ek and Mahrt, 1994), impacts the efficiency of moist convection heat cycle (i.e., the
50 ratio between mechanical work and energy input at the surface; Shutts and Gray, 1999) and the distribution of shallow convec-
51 tion cloud base mass flux (Sakradzija and Hohenegger, 2017). One thus might expect different boundary layer characteristics in
52 surface-forced pre-monsoon and monsoon conditions due to different Bowen ratios for the two environments. However, Bowen
53 ratio does not seem to affect the updraft intensity in deep convection (Hansen and Back, 2015). Instead, the free-tropospheric
54 conditions, impacted by larger-scale atmospheric dynamics, may affect the strength of convection as measured by parameters
55 such as CAPE, LCL height, or maximum pseudo-adiabatic parcel buoyancy.

56 Present study contrasts pre-monsoon and monsoon environments by analyzing a large set of soundings released from Pune,
57 India, in the semi-arid Western Ghat mountains rain-shadow region. Traditional measures of convective environment are dis-
58 cussed with the emphasis of surface forcing. Since no surface flux information is available for the region where long period
59 soundings were obtained, we use data collected at another location in the rain shadow area to document changes in the Bowen



60 ratio and LCL height between pre-monsoon and monsoon conditions. Subsequently, we discuss two sets of idealized numerical
61 simulations that consider the impact of the surface Bowen ratio on convective development. We argue that model results are
62 broadly consistent with our interpretation of the sounding analysis. A brief summary concludes the paper.

63 2 Observations

64 2.1 Data and Instrumentation

65 Data from radiosonde measurements conducted at Pune ($18^{\circ}31' N$, $73^{\circ}51' E$, elevation 530 m amsl) and measurements from
66 Mahabubnagar ($16.75^{\circ}N$, $78.00^{\circ}E$, elevation 498 m amsl, about 500 km south-east of Pune) are used in this study. Both
67 locations are in the leeward side of Western Ghat mountains in the semi-arid rain-shadow region. Total of 84 soundings from years
68 2010-2014 from Pune, divided into 42 pre-monsoon (March, April, May) and 42 monsoon (June, July, August, September)
69 soundings were analyzed. The Pune soundings are launched irregularly (typically once a week) and they are not part of the
70 daily global sounding network (i.e., they are not available, for instance, from the Wyoming air sounding database; [http://](http://weather.uwyo.edu/upperair/sounding.html)
71 weather.uwyo.edu/upperair/sounding.html). The original data are archived at Indian Institute for Tropical Meteorology (IITM)
72 and they feature high spatial resolution as explained below. Vaisala radiosonde RS92-SGP is used, measuring atmospheric
73 temperature, pressure and humidity. Wind speed and direction (not considered in this study) are obtained by tracking the
74 position of radiosonde using GPS. Launch time is 13:00 IST when the solar insolation is near its peak. The operation takes
75 almost two hours with the radiosonde reaching typically up to 30 km altitude with an ascent rate around 5 ms^{-1} . Data is
76 available at approximately 3 m vertical resolution.

77 Second set of observations are surface flux and tropospheric profiles from the Integrated Ground Observational Campaign
78 (IGOC) at Mahabubnagar, south-east of Pune. Observations were conducted during the transition from pre-monsoon to mon-
79 soon and during the monsoon season of 2011. The latent and sensible surface heat fluxes were measured using eddy covariance
80 sensors located on a meteorological tower at 6 m above surface. In addition to the surface heat flux measurements, a microwave
81 radiometer profiler (MWRP) was also placed about 1.2 km from the tower location. MWRP provides vertical profiles of tem-
82 perature and humidity during the diurnal cycle (Balaji et al., 2017). This information is used to calculate lifting condensation
83 level applying the same method as for the Pune soundings (see the next section).

84 2.2 Analysis of Pune soundings

85 For Pune soundings, thermodynamic parameters such as the potential temperature (θ), equivalent potential temperature (θ_e),
86 water vapour mixing ratio (q_v), relative humidity (RH), cloud water mixing ratio (q_c), parcel buoyancy (B) and cumulative
87 Convective Available Potential Energy ($cCAPE$) were derived using thermodynamic equations and standard procedures as
88 described below. Standard parameters describing convective environment, such as lifting condensation level (LCL), level of
89 free convection (LFC), and level of neutral buoyancy (LNB) were calculated as well.



90 Pressure (p), temperature (T), water vapour mixing ratio (q_v) and relative humidity (RH) of the environment were given as
91 the standard sounding data. Geometrical heights of data levels were obtained by integrating the hydrostatic pressure equation
92 from the surface upwards. Subsequently, the input data were interpolated to a regular vertical grid with a uniform spacing of
93 50 m. A simple adiabatic parcel model was then applied to calculate various parameters describing convective environment.
94 Initial conditions for parcel came from lowest levels available in the sounding, typically corresponding to the near-surface
95 conditions. The potential temperature, water vapour mixing ratio, cloud water mixing ratio and the pseudo-adiabatic buoy-
96 ancancy (B) inside the parcel (i.e., neglecting cloud water which is assumed to convert to precipitation and fall out) were de-
97 rived considering only condensation of water vapor. Condensation was calculated assuming that the parcel maintained water
98 saturation and corresponding latent heating was added to parcel potential temperature. The first level where condensation oc-
99 curred was marked as LCL. The level above LCL where parcel buoyancy became positive was marked as LFC, and the level
100 where parcel buoyancy changed from positive to negative (typically in the upper troposphere) was marked as LNB. Pseudo-
101 adiabatic parcel buoyancy was calculated as $B = g(\Delta\theta_v/\theta_{ve})$ where θ_v and θ_{ve} are virtual potential temperatures of rising
102 parcel and of the environment, respectively, and g is gravitational acceleration. The virtual potential temperature is defined as
103 $\theta_v = \theta(1 + \varepsilon q_v)$, where $\varepsilon = R_v/R_d - 1 \approx 0.61$ and R_v and R_d are gas constants for the water vapour and dry air, respectively.
104 The cumulative CAPE ($cCAPE$) was calculated by vertical integration of the parcel positive buoyancy; it is formally defined
105 as $cCAPE(z) = \int_0^z \max(0, B) dz$. Cumulative CAPE shows how CAPE builds up within a rising pseudo-adiabatic parcel.
106 Note that CAPE is given as $cCAPE(z = LNB)$. In addition, the equivalent potential temperature θ_e was calculated using
107 approximate formula:

$$108 \theta_e = \theta \exp\left(\frac{L}{C_p T} q_v\right) \quad (1)$$

109 where L is latent heat of condensation.

110 3 Results of sounding analysis

111 3.1 Temperature and moisture profiles

112 Figure 1 shows vertical profiles of the potential temperature, water vapor mixing ratio and corresponding relative humidity
113 separated into pre-monsoon and monsoon periods. Panels with the potential temperature profiles also show corresponding
114 LCL levels. The atmosphere exhibits contrasting features during the two seasons that are discussed below.

115 3.1.1 Temperature and moisture profiles and their variability

116 For pre-monsoon conditions, the surface temperature is on average several degrees warmer and water vapor mixing ratio is on
117 average about half of that for monsoon period. The latter is arguably related to the contrasting levels of soil moisture in pre-
118 monsoon and monsoon conditions. The temperature and moisture profiles exhibit less day-to-day variability for the monsoon
119 period. The spread of temperature in middle troposphere in the monsoon environment is about half of that for pre-monsoon.
120 In upper troposphere and lower stratosphere, the differences are smaller. For the pre-monsoon period, moisture profiles below

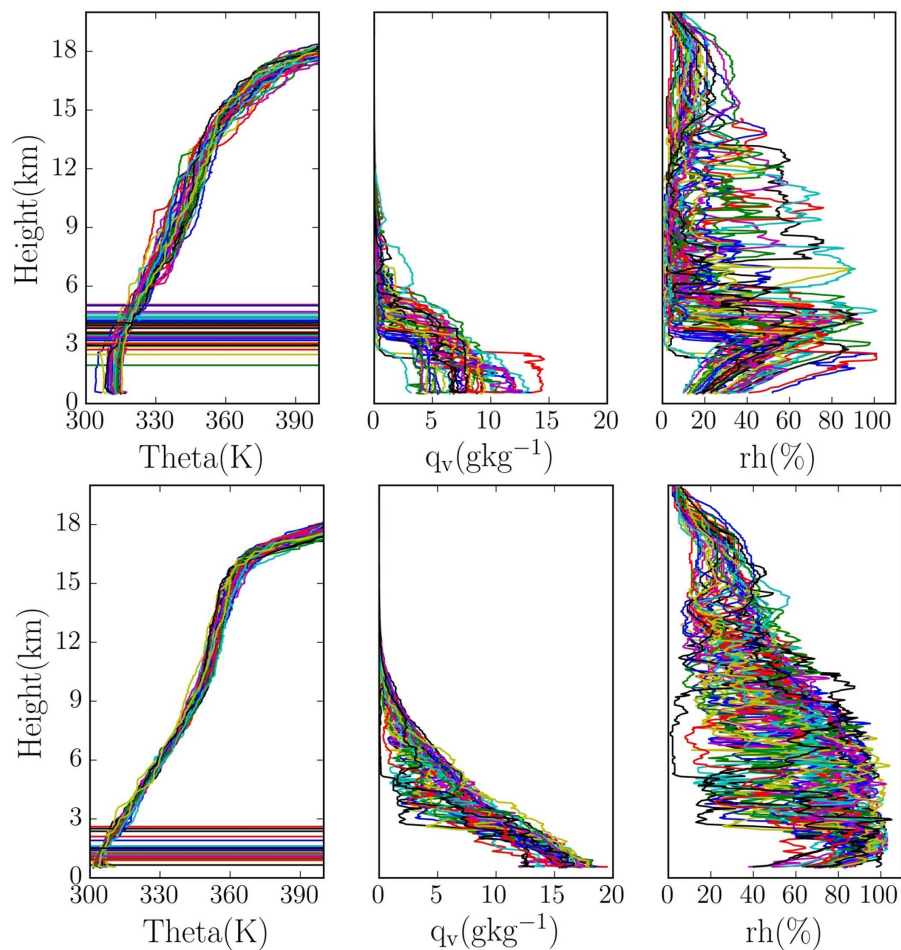


Fig. 1. Profiles of potential temperature (left panels), water vapor mixing ratio (middle panels), and relative humidity (right panels) for pre-monsoon (upper row) and monsoon (lower row) soundings.

121 6 km vary significantly and atmosphere is significantly drier above 6 km when compared to monsoon soundings. Arguably,
122 higher moisture contents in the middle and upper troposphere during monsoon come from convection reaching higher levels
123 as documented later in the paper. However, differences due to large-scale horizontal advection may play some role as well.

124 Individual moisture profiles feature significant fluctuations, even more apparent if no smoothing is applied to the original
125 high resolution data. This is evident at lower levels (i.e., within the boundary layer) as well as aloft. Fluctuations within
126 boundary layer show that it is not well-mixed for the water vapor in most soundings, especially for monsoon conditions.
127 However, relative humidity does increase approximately linearly within the boundary layer in most profiles similar to the case
128 of well-mixed mixed boundary layer (i.e., featuring constant with height potential temperature and water vapor mixing ratio).



129 3.1.2 LCL/boundary layer height

130 In surface-driven convective situations and mid-day conditions with either shallow or deep convective clouds above boundary
131 layer, LCL height should be relatively close to boundary layer height as noted by Balaji et al., 2017 using temperature and
132 moisture profile observations with microwave radiometer profiler. This is because the adiabatic (neutral) temperature profile
133 (i.e., constant θ) within the well-mixed boundary layer has to change to stably-stratified profile (i.e., θ increasing with height)
134 in the free troposphere aloft. Since LCL marks the transition from dry to moist temperature lapse rate within a rising adiabatic
135 parcel, the change from neutral boundary layer and moist-convecting stratified atmosphere aloft should also correspond to
136 LCL. This is consistent with idealized simulations of the diurnal cycle of shallow and deep convection over land (see Brown
137 et al., 2002 and Grabowski et al., 2006, respectively). These simulations show that deepening of boundary layer is accompanied
138 by an increase of LCL height. However, presence of deep convection and significant precipitation can lead to the separation
139 of the well-mixed boundary layer height and LCL height as illustrated later in the paper in idealized simulations (cf., Section
140 5). As Fig. 1 documents, LCLs around 13:00 LST are significantly higher for pre-monsoon period. This may come from either
141 different surface fluxes during the course of the day between pre-monsoon and monsoon periods or from partitioning of the
142 surface energy flux into sensible and latent components. One can argue, however, that the energy passed from earth surface to
143 the atmosphere (the sum of sensible and latent heat fluxes) should be similar in pre-monsoon and monsoon conditions because
144 the solar insolation is similar in both cases. Presence of extensive clouds in monsoon conditions can make a difference for
145 surface energy budget, but we neglect this aspect for the qualitative discussion here. Thus, we assume that development of
146 convective boundary layer during pre-monsoon and monsoon periods is to the leading order affected by partitioning of total
147 surface energy flux into its sensible and latent components, and not by the differences in total flux.

148 The partitioning of surface flux into sensible and latent components depends on the soil moisture that differs drastically
149 between pre-monsoon and monsoon conditions. The surface buoyancy flux that drives boundary layer dynamics is affected
150 by the surface Bowen ratio. Since the thermodynamic variable relevant for buoyancy flux is the virtual potential temperature
151 $\theta_v = \theta(1 + \varepsilon q_v)$, the total surface buoyancy flux BF can be approximated as $BF = \langle w\theta_v \rangle = \langle w\theta \rangle + \theta_o \varepsilon \langle wq_v \rangle$, where
152 θ_o is the surface potential temperature. Total surface energy flux EF can be similarly written (using the moist static energy or
153 the equivalent potential temperature) as $EF = \langle w\theta \rangle + \frac{L}{c_p} \langle wq_v \rangle$. Consequently, BF/EF ratio between the buoyancy and
154 energy surface fluxes can then be represented as:

$$155 \quad BF/EF = (\alpha + B)/(1 + B) \quad (2)$$

156 where $\alpha = \theta_o \varepsilon \frac{c_p}{L} \approx 0.1$ is a numerical coefficient, and $B = \frac{c_p \langle w\theta \rangle}{L \langle wq_v \rangle}$ is the Bowen ratio. For small Bowen ratios (i.e., surface
157 latent heat flux dominates as typically over the oceans) the BF/EF ratio approaches 0.1, that is, only 10 % of the total surface
158 energy flux contributes to the buoyancy flux. For large Bowen ratios (i.e., surface sensible heat flux dominates as over arid and
159 semi-arid areas) the BF/EF ratio approaches 1, that is, all of the total surface energy flux contributes to the buoyancy flux. For
160 Bowen ratio of 1 (i.e., equal surface sensible and latent fluxes), only about half of the energy flux contributes to the buoyancy
161 flux. The equation (2) is shown in Fig. 2. The impact of the surface Bowen ratio on the shallow convective cloud base mass
162 flux has recently been highlighted by Sakradzija and Hohenegger (2017).

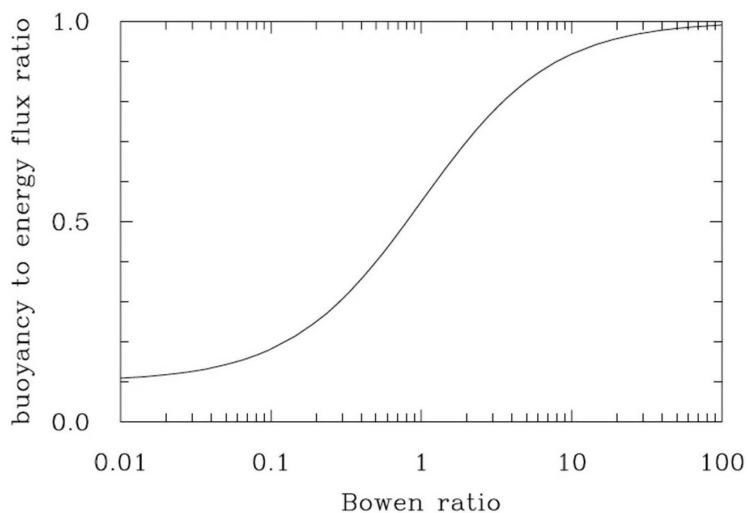


Fig. 2. The ratio of surface buoyancy flux to total energy flux (sensible plus latent) as a function of Bowen ratio.

163 The above considerations explain the well-known fact that daytime convective boundary layer develops deep over arid and
164 semi-arid areas that feature high Bowen ratio due to limited availability of water at the surface. For instance, over the Sahara
165 desert, the boundary layer height can reach several kilometres (e.g., Ao et al., 2012). In contrast, surface-driven convective
166 boundary layer over tropical and sub-tropical oceans is relatively shallow, often a mere several hundred meters. We argue
167 that the differences between pre-monsoon and monsoon periods can, to a large degree, be explained by the availability of soil
168 moisture and partitioning of surface energy flux between sensible and latent components. These differences will be further
169 illustrated by model simulations discussed in section 5.

170 3.1.3 Troposphere-stratosphere transition

171 As Fig. 1 illustrates, the tropopause is much better defined and varies less during monsoon. In contrast, transition from tropo-
172 sphere to the stratosphere is gradual in pre-monsoon environment. This may come from the fact that convection not always have
173 a chance to get to the tropopause in pre-monsoon environment (as documented later in the paper) and other processes (e.g.,
174 large-scale advection or radiative transfer) play an important or even dominant role. A well-defined tropopause is a feature
175 of the monsoon environment. This is associated with the mid tropospheric anticyclone of the Asian monsoon system. Dethof
176 et al. (1999) shows that the upper level monsoon anticyclone located close to tropopause is moistened by the monsoon convec-
177 tion. The strong potential vorticity gradients around tropopause prevent transport across upper-troposphere lower-stratosphere
178 (UTLS) region and result in a strong temperature gradients there. Pune latitude is in the region separating upper level westerlies
179 to the north and easterlies to the south that are associated with mid tropospheric anticyclone.

180 In the case of pre-monsoon conditions, the moisture availability in BL is considerably reduced and this has a significant
181 influence on cloud base height. Air parcels need to rise to greater heights in pre-monsoon conditions to reach LCL compared

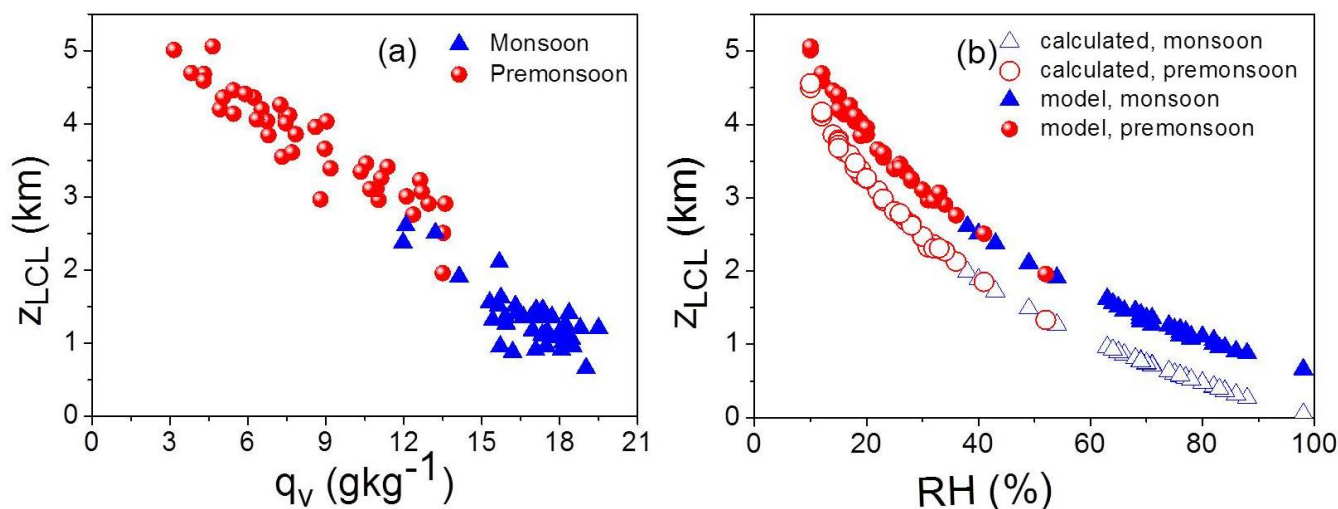


Fig. 3. Variation of LCL height z_{LCL} with (a) surface q_v and (b) surface RH . Red/blue circles/triangles represent pre-monsoon/monsoon cases. Parcel model derived parameters (RH and LCL height) are shown as filled symbols. LCL heights derived using Eq. (3) are shown as empty symbols.

182 to monsoon conditions. Significant variations are observed in LCL heights during these two seasons. Pre-monsoon clouds have
 183 their bases at higher levels, 2 to 6 km from the surface, whereas monsoon soundings indicate cloud bases at lower levels with
 184 most of them being lower than 2 km. This result is highly correlated with surface level moisture as documented below.

185 BL as well as mid-tropospheric moisture for the two seasons exhibit contrasting characteristics. The mean tropospheric
 186 moisture is higher for monsoon soundings. During monsoon, the surface values of q_v are higher compared to pre-monsoon,
 187 and most of them fall within the range of 14-18 gkg^{-1} . Pre-monsoon surface q_v has a lower but wider range from 3 to 14
 188 gkg^{-1} . Monsoon soundings also indicate higher levels of mid-tropospheric moisture. The main reason is south westerly winds
 189 that transport moisture from Arabian Sea to Indian subcontinent. Because of Western Ghat mountains, the transport features
 190 strong low-level convergence over Indian west coast. However, for the inland locations over rain shadow region, the jet core
 191 level is seen at 1.5-2 km, just above the boundary layer. Arguably, boundary layer convection developing during the day pushes
 192 jet layer to an elevated height.

193 3.2 Cloud base height and surface level moisture

194 For a well-mixed boundary layer, water vapor mixing ratio near surface is the main determining factor for cloud base height.
 195 Figure 3 shows the scatterplot of the cloud base height and the surface moisture. Monsoon soundings with higher surface
 196 mixing ratios correspond to lower cloud bases, and pre-monsoon soundings with lower mixing ratios have significantly higher
 197 cloud bases. The relationship between mixing ratio at the surface and cloud base height is approximately linear but with a
 198 significant scatter. However, the relationship between cloud base height and near surface RH is nonlinear, with little scatter.



199 The following simple theoretical analysis explains the tight relationship between surface relative humidity and the cloud
200 base height as shown in Fig. 3. The key assumptions are that the boundary layer is well-mixed and the cloud base is not far
201 from boundary layer top. The two assumptions ensure that air parcels originating from near the surface and reaching LCL
202 insignificantly change their thermodynamic properties during their rise. Overall, these should be valid assumptions in surface-
203 driven convective situations. However, presence of significant precipitation can change this picture as documented later in
204 the paper. When the two assumptions are valid, then the height of the cloud base (i.e., LCL) is the level where adiabatic
205 air parcel rising from surface reaches saturation. If T_{LCL} depicts the LCL temperature and T_s and RH_s depict temperature
206 and relative humidity at the surface, then $q_{vs}(T_{LCL})/q_{vs}(T_s) = RH_s$. Since $q_{vs} \approx e_s/p$ where e_s and p are the saturation
207 water vapor pressure and environmental air pressure, it follows that $e_s(T_{LCL})/e_s(T_s) = p_{LCL}/p_s RH_s$, where p_{LCL} and p_s
208 represent pressure at the LCL and surface, respectively. Applying an approximate Clausius-Clapeyron formula in the form:
209 $e_s(T) = e_0 \exp[\frac{L}{R_v} (\frac{1}{T_0} - \frac{1}{T})]$, where e_0 is the saturated water vapor pressure at the temperature T_0 , leads to: $\frac{1}{T_s} - \frac{1}{T_{LCL}} =$
210 $\frac{R_v}{L} \ln(\frac{p_{LCL}}{p_s RH_s})$. Using the dry-adiabatic relationship between T_{LCL} and T_s in the form $T_{LCL} = T_s - \frac{g z_{LCL}}{C_p}$ gives:

$$211 \ln\left(\frac{p_{LCL}}{p_s RH_s}\right) = -\frac{L g z_{LCL}}{c_p R_v T_{LCL} T_s} \quad (3)$$

212 To show that the relationship is approximately valid for the data used in this study, we derived z_{LCL} from observed p_s , RH_s
213 and T_s , and the parcel model derived p_{LCL} and T_{LCL} . As the figure shows, Equation(3) provides z_{LCL} estimates that are
214 lower than the z_{LCL} calculated from the parcel model, and the difference between z_{LCL} estimated from the parcel model and
215 derived from Equation(3) is typically around 600 meters regardless of the surface humidity.

216 There are at least two explanations for the underestimation of z_{LCL} by Equation(3), both associated with the well-mixed
217 assumption for the boundary layer. The first one has to do with the presence of superadiabatic layer near the surface (i.e., the
218 potential temperature decreasing with height), clearly evident in many soundings shown in Fig. 1. With the surface temperature
219 higher than the mean boundary layer potential temperature, z_{LCL} needs to be higher to keep $z_{LCL}/(T_{LCL} T_s)$ approximately
220 constant on the right-hand-side of (3) as p_{LCL}/p_s can change little. Since 600 m corresponds to about 6 K along the dry adia-
221 batic lapse rate, such an explanation would imply that the air temperature change across the superadiabatic layer is universally
222 about 6 K in the sounding data used here. This does not seem inconsistent with at least some soundings shown in Fig. 1. The
223 boundary layer may also become not well-mixed (i.e., develop moisture and temperature stratification) because of precipitation
224 or low-level horizontal advection, presence of neither is possible to deduce from the available data. In convective situations,
225 significant surface precipitation is always accompanied by convective-scale downdrafts and boundary-layer cold pools. Since
226 the air in a cold pool typically comes from middle troposphere, the low-level water vapor mixing ratio inside the cold pool is
227 typically lower than on the outside (e.g., Tompkins, 2001). In such a situation, the boundary layer cannot be assumed well-
228 mixed and entrainment of boundary-layer air into a plume rising from surface would lead to plume dilution and thus to the
229 increase of LCL height. Moreover the parcel model constitutes a significant simplification of real atmosphere in which the
230 sonde is flown taking a Lagrangian path and cutting across different air columns.

231 The above analysis is consistent with results discussed in Murugavel et al. (2016). They showed that the column precipitable
232 water (PW), the vertical integral of water vapor density in the atmosphere, is a good predictor of LCL temperature and height



233 over the Indian subcontinent. Since the column PW is dominated by moisture in the lowest levels (and in the boundary layer
234 in particular), the mixing ratio near the surface should then be well correlated with LCL height as documented in Fig. 3.

235 The above results can also be used in reverse. The fact that, despite some offset, there is an almost a perfect relationship
236 between RH and z_{LCL} implies that mid-day boundary layer for all soundings considered in this study is of convective type,
237 that is, with close to the adiabatic potential temperature profile from above the superadiabatic surface layer up to the convective
238 boundary layer height and LCL.

239 3.3 Profiles of pseudo-adiabatic buoyancy and cCAPE

240 CAPE represents the energy available for moist convection and larger values of CAPE indicate larger potential for strong con-
241 vection. Figure 4 shows profiles of pseudo-adiabatic buoyancy (i.e., the difference in the virtual potential temperature between
242 pseudo-adiabatic parcel and the environment) and cCAPE from all soundings separated into pre-monsoon and monsoon con-
243 ditions. In addition, pre-monsoon soundings are divided into three groups (marked by red, blue, and green lines in left panels)
244 depending on CAPE values, with red/blue/green colors corresponding to low/medium/high CAPE values. This partitioning
245 will be used in the subsequent analysis. Monsoon and pre-monsoon environments exhibit distinct patterns. First, there is a
246 significant day-to-day variability for both environments as marked by the spread in profiles, but the variability seems larger
247 for pre-monsoon conditions. The variability is affected mostly by the surface water vapor mixing ratio as quantified later in
248 the paper. Large CAPE pre-monsoon soundings (green colour) are characterized by pseudo-adiabatic parcel maximum buoy-
249 ancies that are not different from their monsoon counterparts, but LNBs and CAPE values (evident from end points of cCAPE
250 profiles) are typically lower for the pre-monsoon environment.

251 Most of the monsoon pseudo-adiabatic buoyancy and cCAPE profiles follow a consistent pattern, as shown in right panels of
252 Fig. 4. These soundings maintain positive pseudo-adiabatic buoyancies up to the upper troposphere with CAPE values typically
253 between 1000 and 2000 Jkg^{-1} , except for a few cases. This is different for pre-monsoon soundings that feature wide range
254 of maximum in-cloud buoyancies, with three distinct branches. The first branch represented by green lines follows a pattern
255 similar to monsoon cases, but with lower CAPE values and lower LNBs. The second branch, marked by blue lines, represents
256 intermediate soundings with CAPE typically between 500 and 1000 Jkg^{-1} , and LNBs typically in middle troposphere. Red
257 lines represent the cases with low CAPE and LNB located in lower or middle troposphere.

258 These results show that monsoon season feature convective environments that are all similar and can be grouped into a
259 single family. In contrast, pre-monsoon season witnesses a wide range of atmospheric conditions and convection with diverse
260 properties, from situations with low-CAPE and LNBs in the lower and middle troposphere to situations with CAPE comparable
261 to monsoon environments and LNBs in the upper troposphere. One distinct feature of high-CAPE pre-monsoon category is that
262 the positive buoyancy increases steeply above LFC compared to the monsoon cases where buoyancy increased gradually above
263 the boundary layer. This is possibly due to the stark difference in moisture above LFC between pre-monsoon and monsoon
264 environments and its impact on the pseudo-adiabatic buoyancy.

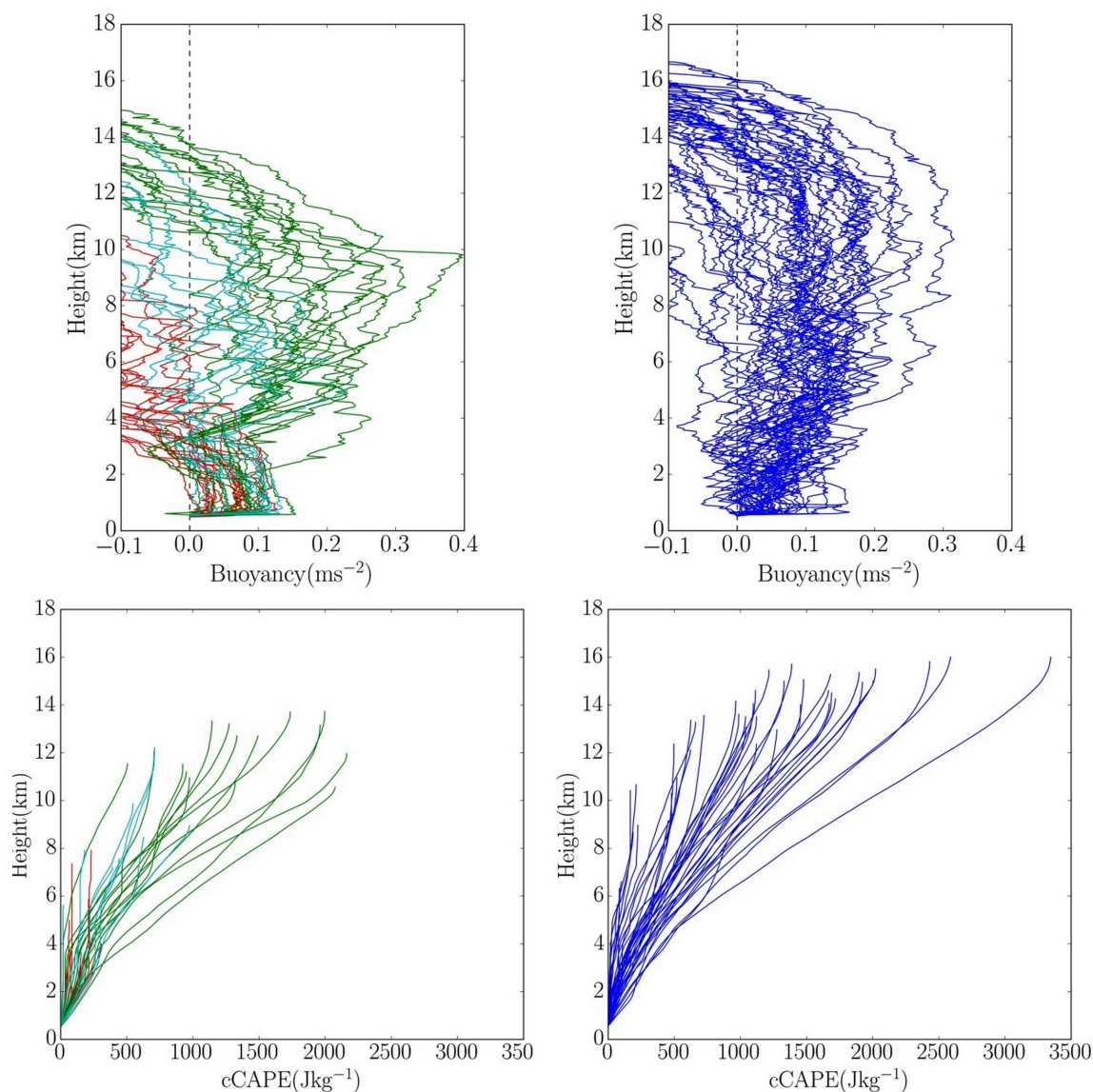


Fig. 4. Profiles of the pseudo-adiabatic buoyancy (upper panels) and cCAPE (lower panels) for pre-monsoon (left column) and monsoon (right column) soundings. cCAPE profiles terminate at LNB. Pre-monsoon soundings are divided into three groups marked by red, light blue and green lines depending on the CAPE value.

265 3.4 CAPE, LNB and maximum buoyancy as a function of surface conditions

266 Figure 5 relates CAPE and LNB to the surface water vapor mixing ratio q_v . Using surface relative humidity instead of q_v
267 gives similar results (not shown). Despite significant scatter, the clear pattern is evident: low q_v pre-monsoon environment is
268 associated with the lowest LNB and CAPE, with q_v as low as a quarter of the high-CAPE monsoon cases. Gradual increase of

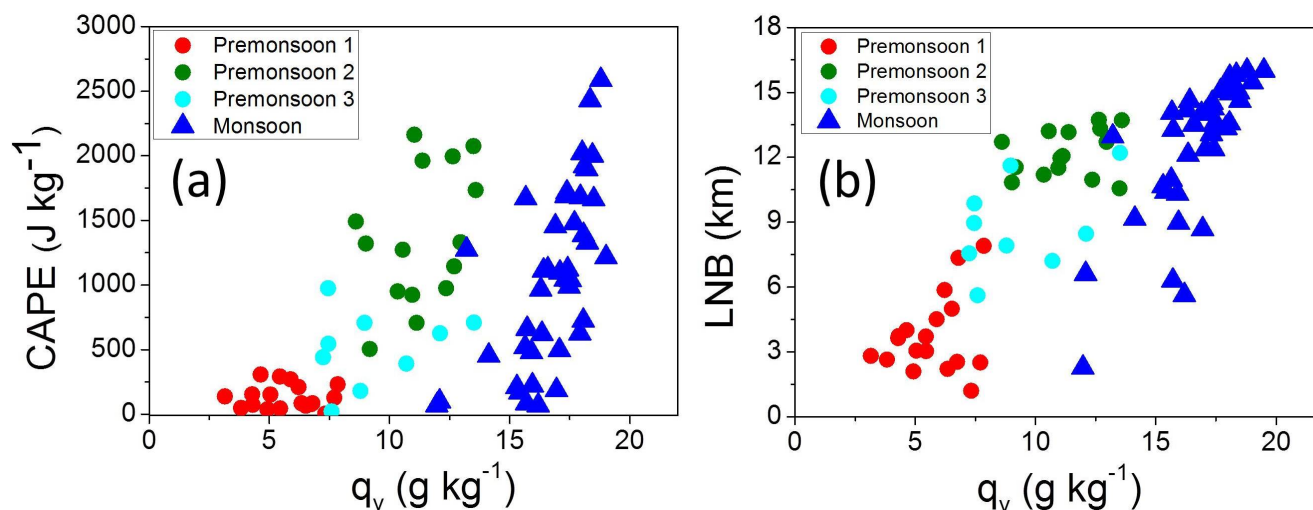


Fig. 5. Variation of (a) CAPE and (b) LNB as a function of surface water vapor mixing ratio. Pre-monsoon cases are grouped similarly as in Fig. 4

269 q_v in pre-monsoon cases leads to gradual increase of CAPE and LNB. High CAPE and LNB monsoon cases are associated with
 270 high surface q_v . The increase of CAPE with surface humidity is consistent with results reported in Alappattu and Kunhikrishnan
 271 (2009), who analysed pre-monsoon observations over oceanic region surrounding the Indian subcontinent (cf., Fig. 8. therein).
 272 Our study also supports findings of Bhat (2001), who reported that CAPE over Bay of Bengal during monsoon season varies
 273 linearly with mixed layer specific humidity (cf., Fig. 3 therein). In our analysis, the linear relationship between surface q_v and
 274 CAPE is well defined for monsoon season, arguably because of the small free-troposphere temperature variations (cf., Fig. 1)
 275 and small variations of LNB (Fig. 5b). Pre-monsoon convective environments exhibit larger scatter, arguably because of larger
 276 variability of temperature profiles (Fig. 1) and LNBs (Fig. 5b).

277 Figure 6 shows the maximum pseudo-adiabatic parcel buoyancy as a function of surface water vapor mixing ratio, q_v (panel
 278 a) and the surface equivalent potential temperature, θ_e (panel b). Circles (triangles) mark pre-monsoon (monsoon) conditions
 279 and the symbol colour depicts cloud base height according to the color scale shown to the right of the panels. Overall, neither
 280 surface q_v nor surface θ_e is a good predictor of the parcel maximum buoyancy. The maximum buoyancy does seem to increase
 281 with the surface q_v , but the relationship is rather weak and there is a large scatter. The scatter reduced while soundings with
 282 similar cloud base heights are considered.

283 The most apparent pattern, already discussed in section 3.2, is that the surface q_v strongly affects the cloud base height. The
 284 main contrast between pre-monsoon and monsoon conditions comes from contrasting relationship in low-level temperature
 285 and humidity, that is, higher temperature and lower humidity for pre-monsoon cases, lower temperature and higher humidity
 286 for monsoon cases. Because of compensating effects of the temperature and humidity on θ_e , its surface values is thus not a
 287 good predictor of the maximum pseudo-adiabatic parcel buoyancy either.

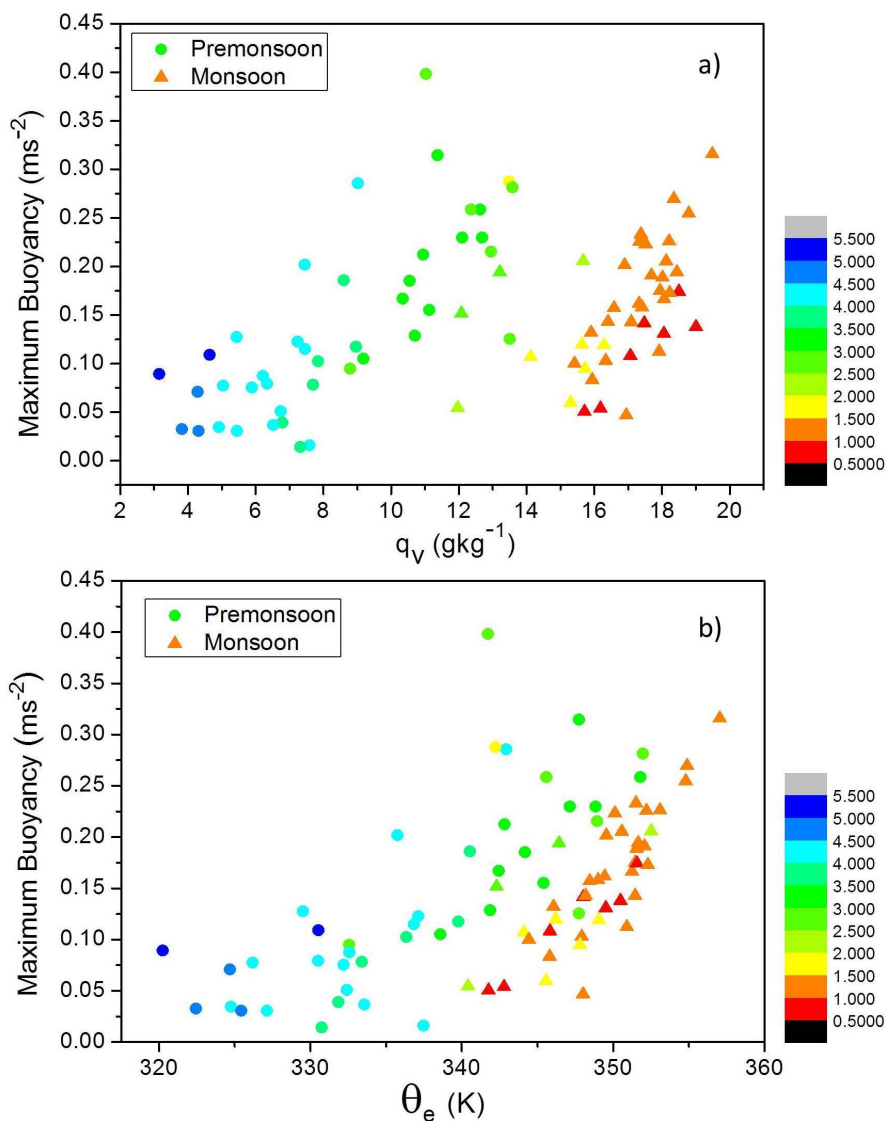


Fig. 6. Variation of the maximum quasi-adiabatic buoyancy as a function of (a) surface water mixing ratio and (b) surface equivalent potential temperature. Triangular/circular symbols are for monsoon/pre-monsoon soundings, with the color depicting the cloud base height. Pre-monsoon cases are grouped as in Fig. 4 and 5.

288 In summary, the availability of surface moisture seems to be a significant determinant of deep convection development
289 over Indian subcontinent (assuming that conditions near Pune can be taken as a representative for the rain shadow region),
290 with pre-monsoon and monsoon conditions providing contrasting examples of the impact. Day-to-day variability of surface
291 moisture is larger during pre-monsoon season and it adds to the variability associated with free-tropospheric conditions, such
292 as temperature and moisture stratification.



293 **4 Observations of surface forcing during the pre-monsoon to monsoon transition**

294 Since surface flux observations are not available simultaneously with Pune sounding data, we use observations collected during
295 IGOE campaign to contrast the role of surface forcing between pre-monsoon and monsoon conditions. As explained in section
296 2.1, IGOE tower measurements of surface sensible and latent heat fluxes are combined with the estimates of LCL using
297 MWRP-derived lower-tropospheric temperature and moisture profiles. Figure 7 shows evolutions of surface fluxes, Bowen
298 ratio, and LCL height between June 24 and end of July using 3-hourly data during the diurnal cycle. Pre-monsoon to monsoon
299 transition (monsoon onset hereafter) around July 1st is clearly evident in the figure. Before the monsoon onset, sensible heat
300 flux is typically much larger than latent flux, and Bowen ratio is larger than 1. After monsoon onset, latent and sensible fluxes
301 reverse, with latent heat flux becoming much larger than the sensible flux and Bowen ratio becomes smaller than one. The
302 LCL height seems to decrease as Bowen ratio decreases after the monsoon onset and diurnal variations of LCL height become
303 less significant after the monsoon onset. There seems to be a weak decreasing trend in the evolutions of Bowen ratio and LCL
304 height after the monsoon onset, arguably consistent with the gradual increase of soil moisture during monsoon.

305 Although IGOE flux data shown here are for a single monsoon onset case, in contrast to 5 years of sounding data, the
306 transition from the high-Bowen ratio pre-monsoon environment to the low-Bowen ratio monsoon environment is fairly typical
307 over Indian subcontinent. The impact of surface Bowen ratio on the evolution of monsoon deep convection is further illustrated
308 by numerical simulations discussed in the next section.

309 **5 Simulations of deep convection driven by surface forcing**

310 Two sets of idealized simulations of moist convection with emphasis on the surface forcing are discussed in this section in
311 support of analysis presented previously. The first pair of simulations considers monsoon convection applying two specific
312 mid-day soundings from IGOE field project, one corresponding to relatively moist surface conditions and second one for dry
313 condition. The soundings are from the period toward the end of monsoon, 18th September (wet case) and 2nd October (dry
314 case). As already explained, the soundings come from radiosonde released about 1.2 km away from surface flux tower site.
315 The simulations are idealized because they apply mid-day sounding as initial condition and use mid-day observed surface
316 conditions to calculate surface fluxes, driving the several-hour-long simulations. In reality, surface conditions change because
317 of the diurnal variations of surface insolation.

318 Because of such a limitation, we employ a second set of simulations that considers a daytime convective development from an
319 early morning sounding driven by evolving surface fluxes. The simulations are based on observations in the South American
320 Amazon region (Grabowski et al., 2006). As an illustration, we introduce a simple modification of the surface Bowen ratio
321 and analyze its impact. Although also idealized (i.e., prescribed horizontally-uniform surface fluxes), the simulations provide
322 additional illustration of the role of surface forcing for deep convection development.

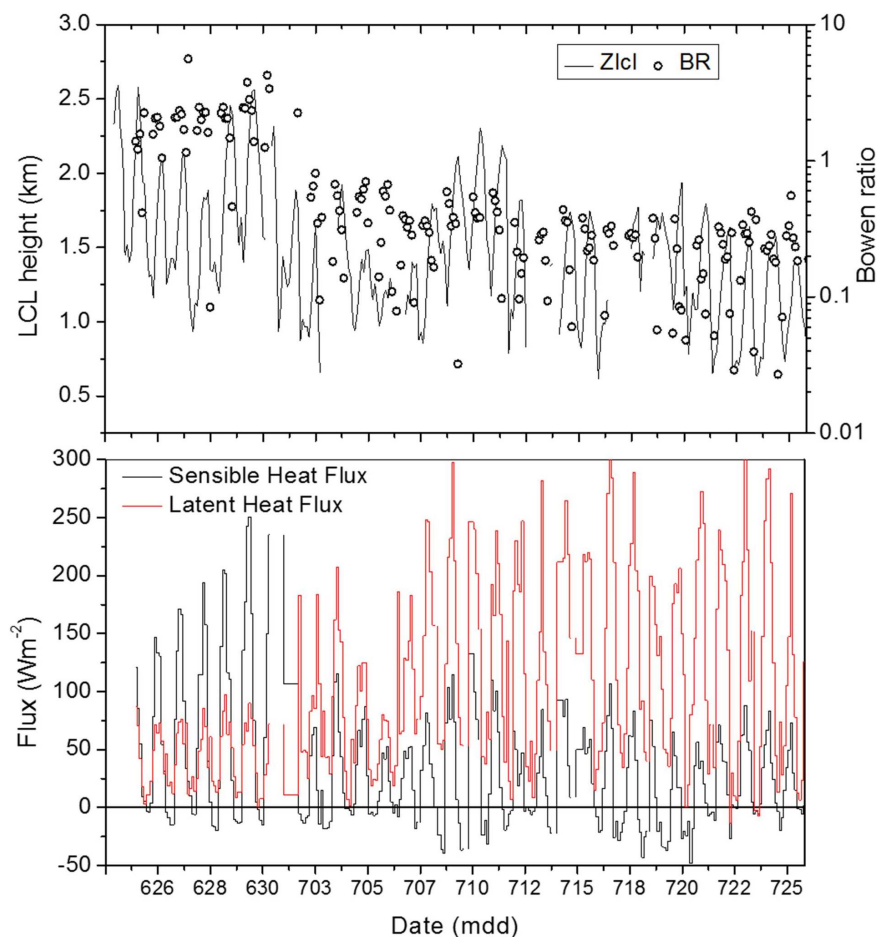


Fig. 7. Evolutions of (upper panel) Bowen ratio (BR) and LCL height (Z_{lcl}) and (lower panel) sensible (black lines) and latent (red lines) surface heat fluxes around the monsoon onset from the IGOc data.

323 5.1 Two IGOc cases of monsoon convection over India

324 Two contrasting soundings, referred to as wet and dry, were collected as the southwest monsoon was receding from Indian
325 subcontinent and the lower atmosphere was getting progressively dry. The wet case is September 18th and the dry case is
326 October 2nd. Soundings on both days were conducted around noon local time. The surface potential temperature and water
327 vapor mixing ratio for the wet case were 305.2 K and 16.6 gkg⁻¹. Corresponding values for the dry case were 306.1 K and
328 13.5 gkg⁻¹. The contrasting surface temperature and moisture has been the determining factor for selecting these two cases.

329 Figure 8 compares the two soundings. Wet sounding features about 1 km deep mixed layer (although with a noticeable
330 vertical moisture gradient) and relatively uniform free-tropospheric stability aloft. In contrast, dry sounding features no mixed
331 layer near the surface, and a fairly complex structure in the lowest 5 km with distinct layers of approximately constant stability:

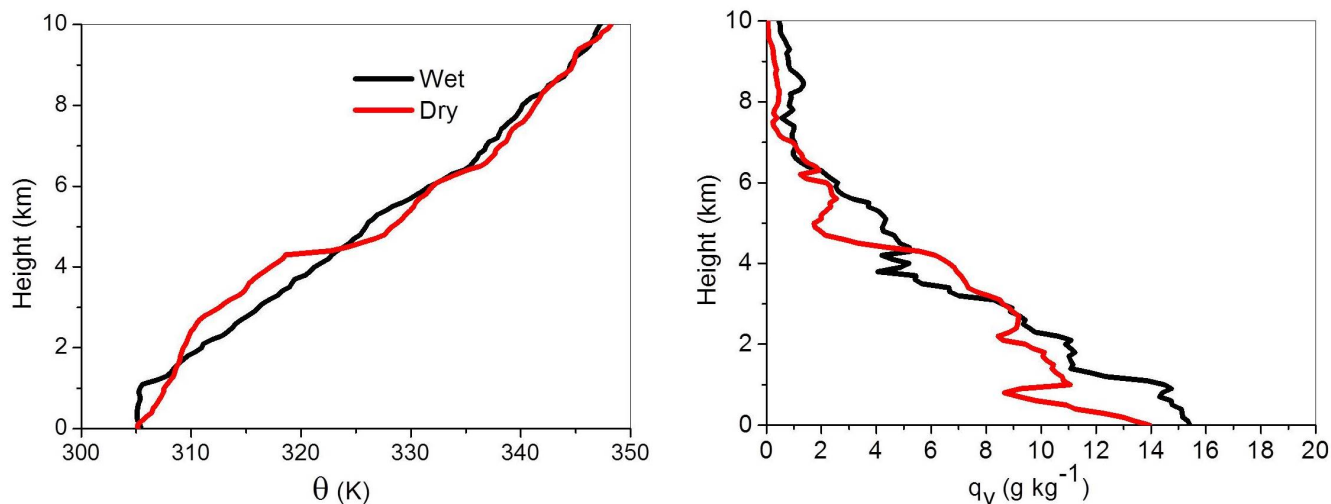


Fig. 8. Vertical profile of potential temperature and water vapour mixing ratio used in the simulations for wet and dry cases from the IGOE field project.

332 weakly stratified layer between the surface and about 3 km, typically-stratified layer between 3 and approximately 4.5 km, and
333 an inversion between 4.5 and 5 km. The wet case has higher wind speed (greater than 4 ms^{-1} ; not shown) compared to the
334 dry case (smaller than 3 ms^{-1}). The mid-tropospheric inversion provides a barrier for deep convection as illustrated by model
335 results. LCL height for the wet case is around 1.1 km, significantly lower than that for the dry case (around 1.6 km) due to
336 moisture availability near the surface.

337 The model used for the two case simulations is the NCAR Weather Research and Forecasting (WRF) model (Skamarock
338 et al., 2005) ran in the LES mode. The horizontal domain of 20 by 20 km^2 applies the 100 m grid length. The 10-km deep
339 vertical domain is covered with a uniform grid with a 50-m vertical spacing. The model is run in an idealized manner for 8 hours
340 applying surface fluxes derived from initial prescribed constant surface temperature and moisture values. Since the simulations
341 start with horizontally-uniform conditions and require spin-up time to develop small-scale circulations and clouds, we present
342 model results starting from hour 3. Figure 9 shows evolution of surface sensible and latent heat fluxes and Bowen ratio between
343 hours 3 and 8. The sensible heat fluxes change little during the simulations, but latent fluxes decrease significantly, especially
344 in the dry case. The initial total surface heat flux is about 20 Wm^{-2} larger in the wet case and the difference increases
345 as simulations progress. This implies that the surface total heat flux is larger in wet case and the difference between two
346 simulations increases with time. The Bowen ratio is approximately 2 at the onset of two simulations. It remains close to 2 for
347 the wet simulation, but increases to values around 12 at hour 8 for the dry case.

348 For the wet case, initial sounding features already a well-identifiable mixed layer (at least for the potential temperature),
349 and the surface energy and the Bowen ratio change little throughout the simulation. Thus, the boundary-layer height increases
350 steadily throughout the simulation, as shown in Fig. 10. The increase of boundary layer height in the wet case is accompanied
351 by the increase of cloud base height. The depth of the cloud field, however, increases at a higher rate, from about 2.5 km at

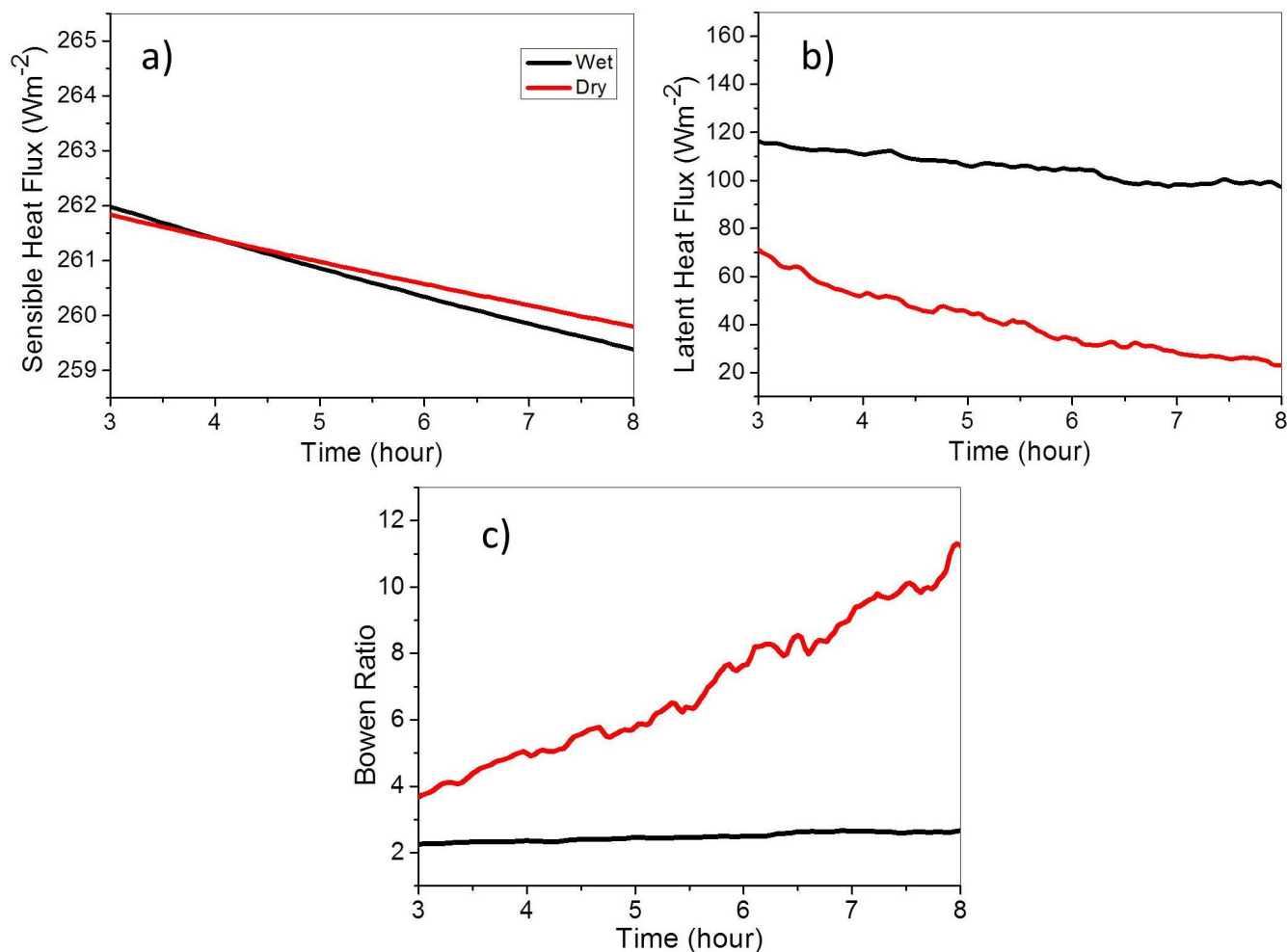


Fig. 9. Evolution of (a) sensible heat flux, (b) latent heat flux, and (c) Bowen ratio in simulations of dry and wet cases from the IGOc field project. Red/black lines are for dry/wet case.

352 hour 3 to about 5 km at hour 8. For the dry case, mixed layer is absent in the initial sounding, and thus it rapidly develops
353 during the initial couple hours of the simulation. Boundary layer depth is about 1 km at hour 1 (not shown) and about 2.2 km
354 at hour 3. The rate then decreases significantly and boundary layer deepens subsequently at a rate comparable to the wet case,
355 about 100 m per hour. The cloud base height rises at a similar rate, and cloud field depth remains quite steady at around 2 km
356 between hours 3 and 8. The presence of a deep inversion between 4.5 and 5 km (see Fig. 9) provides an efficient lid for the
357 convective development.

358 The changes in cloud field between hour 5 and 8 are illustrated in Fig. 11 that shows corresponding cloud fraction profiles
359 for the two simulations. The figure illustrates increase of cloud base heights with time that are similar for dry and moist cases,

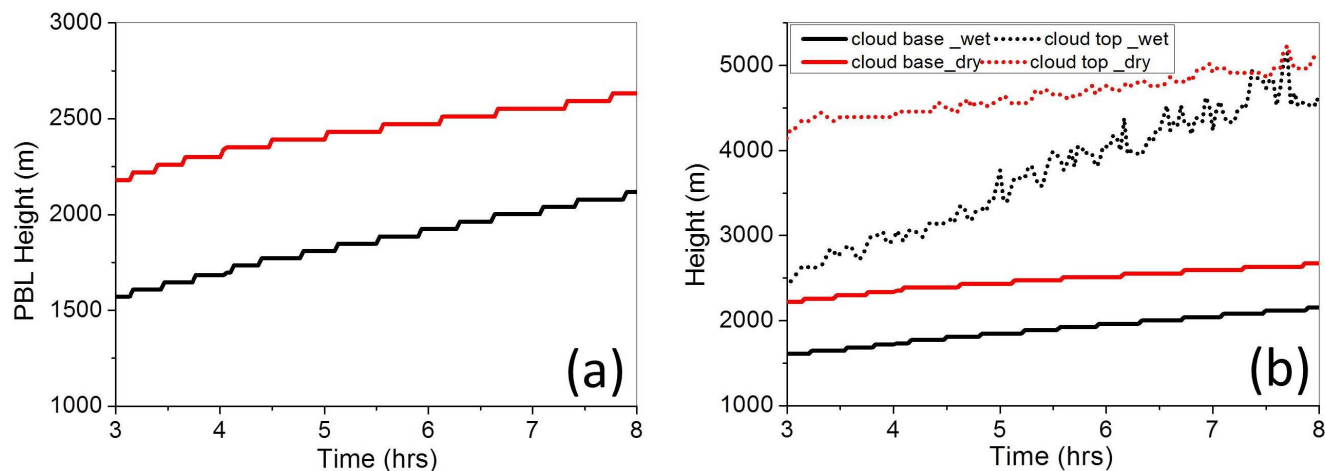


Fig. 10. Evolution of (a) PBL height and (b) cloud base and cloud top heights from dry and wet simulations of the IGOE field project. Red/black lines are for dry/wet case.

360 a significant deepening of the cloud field in moist case, and the impact of inversion between 4.5 and 5 km for the dry case that
 361 results in almost 100 % cloud cover within the inversion.

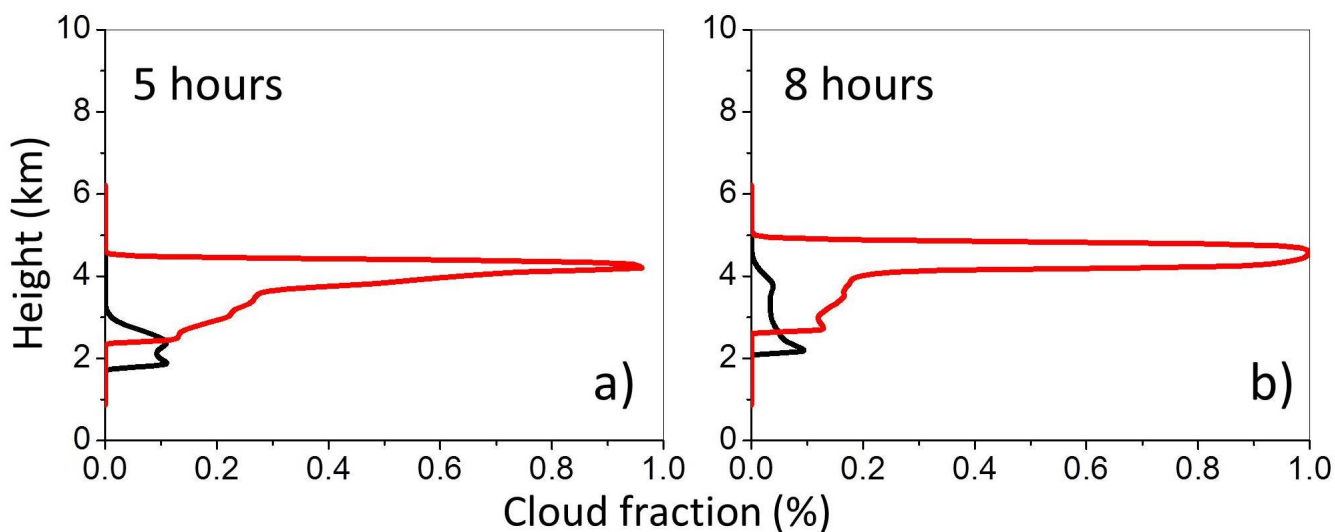


Fig. 11. Cloud fraction profiles at (a) hour 5 and (b) hour 8 from dry and wet simulations of the IGOE field project. Red/black lines are for dry/wet case.

362 In summary, high-resolution simulations of contrasting realistic cases observed over Indian subcontinent illustrate the impact
 363 of surface forcing and highlight the role of specific free-tropospheric conditions for convective development and cloud fraction.



364 The latter are no doubt responsible to some spread of the observed convective environments apparent in Pune sounding data
365 analyzed in section 3.

366 **5.2 Idealized simulations of daytime convective development over land: the LBA case**

367 Since the first set of simulations applied highly idealized forcing, we use another pair of simulations that aim at simulating
368 daytime convective development over land, starting from the cloud-free morning sounding and finishing with the mid-day deep
369 convection. We apply the case developed in Grabowski et al. (2006) where observations from Amazon region motivated the
370 design of a simple modeling case. The case features formation and deepening of the cloud-free convective boundary layer in
371 the early morning hours, development of shallow convection in the late morning, and transition to deep convection around the
372 local noon. The 6-hour simulation covers period from 7.30 am local time (approximately at the sunrise) to the mid-day hours
373 (1.30 pm local time). It starts from horizontally-homogeneous morning sounding and is forced by increasing surface latent and
374 sensible heat fluxes mimicking effects of the increasing daytime surface insolation. This case has been used in several past
375 studies, such as Khairoutdinov and Randall (2006), Grabowski (2015) and Grabowski and Morrison (2016, 2017). We apply
376 the microphysical setup based on Grabowski (1999), that is, the one referred to as IAB in Grabowski (2015).

377 Two simulations are performed. The first simulation, referred to as LBA, follows original setup and features significantly
378 larger surface latent flux compared to the sensible flux, with the Bowen ratio between 0.4 and 0.5 as the surface fluxes evolve
379 (this is similar to wet cases during the Indian monsoon season). Surface fluxes are switched in the second simulation, that is,
380 the sensible flux takes values of the latent flux and the latent flux assumes values of the sensible flux. This simulation is referred
381 to as reversed LBA, or R-LBA, and it features the surface Bowen ratio between 2.0 and 2.5. According to Fig. 2, such a change
382 approximately doubles the buoyancy to energy flux ratio, from about 0.4 to about 0.7. One thus should expect significantly
383 deeper boundary layer to develop during the course of the R-LBA simulation.

384 The model used in the two simulations is the same as in Grabowski (2015) and Grabowski and Morrison (2016, 2017),
385 referred to as babyEULAG, a simplified version of the EULAG model (see <http://www2.mmm.ucar.edu/eulag/>). Since the
386 interest is in the boundary layer development, we apply a higher horizontal resolution with horizontal grid length of 200 m and
387 the same stretched vertical grid as in Grabowski (2015) and Grabowski and Morrison (2016, 2017). The horizontal domain
388 is 24 x 24 km². Overall, one can argue that differences between LBA and R-LBA towards the end of the simulation should
389 be relevant to the differences in the mid-day soundings between dry pre-monsoon and humid monsoon situations discussed
390 earlier.

391 Figure 12 and Fig. 13 summarize results of the two simulations pertinent to the impact of the surface flux Bowen ratio on
392 convective development. Figure 12 shows profiles of the cloud fraction in 1 hour intervals from 6-hour long LBA and R-LBA.
393 Overall, the profiles evolve in a quite similar way, with only shallow clouds at hour 2 and 3, and deep convection present at hour
394 5 and 6. The profiles at hour 4 correspond to the shallow-to-deep transition period. The differences in the cloud base height
395 in the simulations are apparent, with R-LBA (higher Bowen ratio) featuring higher mean cloud base. Figure 13 shows the
396 evolution of the mean cloud base height together with the evolution of the estimated height of the boundary layer. As the figure
397 shows, boundary layer depth is up to twice as deep in the R-LBA case than in the LBA case, especially between hours 2 and

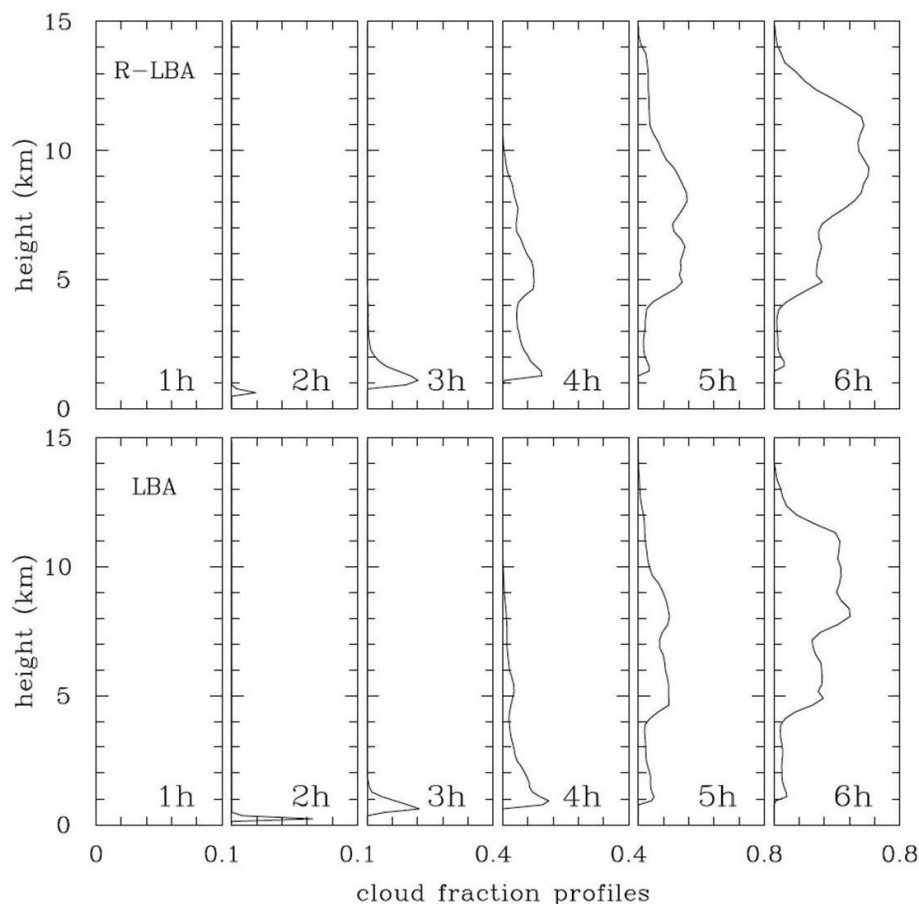


Fig. 12. Cloud fraction profiles at hour 1, 2, 3, 4, 5, and 6 from (upper panels) R-LBA and (lower panels) LBA simulations.

398 3 and during the hour 5 of these simulations. The cloud base height and the height of the boundary layer top track each other
399 well up to the onset of a significant precipitation after hour 3. The difference between the two heights is especially evident in
400 the LBA case as boundary layer height changes little during the two final hours. Specific differences between LBA and R-LBA
401 in the last two hours of the simulations may not be statistically significant due to the small domain size.
402 Overall, differences simulated in LBA and R-LBA cases highlight the impact of surface flux Bowen ratio and provide additional
403 support for its role in the difference between pre-monsoon and monsoon soundings.

404 6 Summary

405 Thermodynamic soundings released around local noon for several pre-monsoon and monsoon seasons over Indian subcontinent
406 were analysed. Various parameters, such as pseudo-adiabatic parcel buoyancy, Lifting Condensation Level (LCL), Level of
407 Free Convection (LFC), Level of Neutral Buoyancy (LNB), Convective Available Potential Energy (CAPE), cumulative CAPE

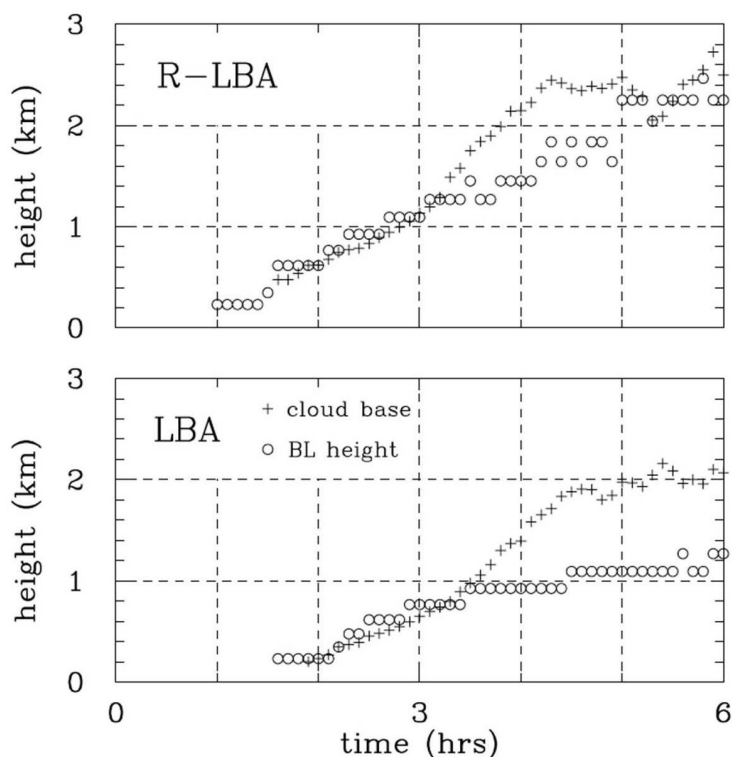


Fig. 13. Evolution of the cloud base height (plus signs) and the boundary layer height (circles) in R-LBA (upper panel) and LBA (lower panel) simulations. Dashed line are included to highlight differences between the simulations.

408 (cCAPE) were derived applying pseudo-adiabatic parcel model. Overall, pre-monsoon soundings show more variability of
409 surface and free-tropospheric conditions as documented in Fig. 1. For surface, the key is availability of surface moisture in both
410 pre-monsoon and monsoon environments, whereas variability of free tropospheric temperature and humidity for pre-monsoon
411 is arguably because of the impact of factors other than deep convection itself, for instance, the large-scale dynamics.

412 The pre-monsoon soundings feature higher cloud bases than monsoon soundings. We argue that this is a consequence of
413 partitioning of surface energy flux into its sensible and latent components as expressed by the Bowen ratio. For large Bowen
414 ratios (sensible surface flux is much larger than latent flux), the ratio between the buoyancy to energy flux is close to one, that
415 is, all surface flux contributes to buoyancy flux that drives boundary layer dynamics. For small Bowen ratios (i.e., sensible
416 surface flux much smaller than latent flux), only about 10 % of the energy flux is used for surface buoyancy flux (see Fig. 2).
417 We argue that the partitioning of surface energy flux into its sensible and latent components determines variations in the LCL
418 height as illustrated by observed rapid changes in Bowen ratio and LCL height near monsoon onset and illustrated in idealized
419 numerical simulations. Observations of LCL height and Bowen ratio during the pre-monsoon to monsoon transition illustrate
420 rapid and concurrent changes, with the Bowen ratio and LCL height decreasing significantly as the monsoon sets in. The impact



421 of surface forcing on the evolution of boundary layer and moist convection is also illustrated through numerical simulations
422 that complement sounding analysis.

423 The sounding data show that LCL height is linearly related to surface level moisture content with some scatter around the
424 perfect linear relationship (Fig. 3a). The scatter is eliminated when surface level relative humidity (RH) is used as a measure
425 of surface layer moisture content (Fig. 3b). A theoretical basis for such a relationship is developed, see Eq. 3. The theoretical
426 relationship between LCL height and surface level RH mimics the relationship obtained with the parcel model. However, a
427 significant offset is present between the theoretical LCL height and LCL predicted by the parcel model. The offset is argued
428 to most likely come from the presence of surface superadiabatic layer not considered in the theoretical argument. The general
429 consistency between theoretical and parcel-model derived relationships between LCL height and surface moisture (Fig. 3)
430 supports the conjecture that surface forcing determines LCL height. This should be expected in high-insolation pre-monsoon
431 and monsoon conditions when surface forcing due to diurnal cycle drives formation of well-mixed convective boundary layer
432 in the morning and development of deep convection at later hours.

433 Overall, LNB and CAPE vary more for the pre-monsoon soundings. Large CAPE pre-monsoon soundings are characterized
434 by maximum pseudo-adiabatic parcel buoyancies that are similar to monsoon soundings. With a few monsoon exceptions,
435 low LNB and thus low CAPE soundings are present only for pre-monsoon environment. For both pre-monsoon and monsoon
436 soundings LNB and CAPE are linearly related to surface q_v with a larger scatter for the pre-monsoon environment. In general,
437 neither surface q_v nor surface θ_e are good predictors of the parcel maximum pseudo-adiabatic buoyancy, although there is a
438 general increase of the maximum buoyancy and CAPE with the increase of either the surface q_v or θ_e . The increase is along
439 different paths for pre-monsoon and monsoon soundings, see Fig. 4 and 5. The scatter is small for monsoon cases, no doubt
440 because of smaller variability of free-tropospheric structure as documented in Fig. 1.

441 Results presented in this paper should help understanding effects of aerosols, dramatically different between highly-polluted
442 pre-monsoon environment and relatively clean environment during the monsoon, on moist convection over Indian subcontinent.
443 Understanding dynamical effects, for instance, partitioning of the surface heat flux into its sensible and latent components and
444 how the partitioning affects cloud base height and cloud buoyancy, is required for a confident selection of deep convection
445 cases suitable for cloud seeding, the target of the ongoing Indian precipitation enhancement program (Prabha et al., 2011;
446 Kulkarni et al., 2012; Prabha, 2014).

447 *Acknowledgements.* This work was done as part of SN Bose Scholarship program (Indo-US Student Exchange program by IUSSTF) at
448 National Center for Atmospheric Research (NCAR) and M. Tech project work at Indian Institute of Tropical Meteorology (IITM). First
449 author thanks Department of Atmospheric and Space Sciences, Savitribai Phule Pune University for nominating to SN Bose Scholarship
450 program, and acknowledges NCAR and IITM for providing facilities to conduct the study. CAIPEEX experiment was funded by Ministry
451 of Earth Sciences. Authors acknowledge field contributions from several colleagues of Indian Institute of Tropical Meteorology, Pune in
452 collection of data used in this study. WWG was partially supported by the Polish National Science Center (NCN) “POLONEZ 1” Grant
453 2015/19/P/ST10/02596. The POLONEZ 1 grant has received funding from the European Union’s Horizon 2020 Research and Innovation



454 Program under the Marie Skłodowska-Curie Grant Agreement 665778. WWG acknowledges IITM financial support and hospitality during
455 his visits to IITM.



456 References

- 457 Alappattu, D. P. and Kunhikrishnan, P.: Premonsoon estimates of convective available potential energy over the oceanic region surrounding
458 the Indian subcontinent, *Journal of Geophysical Research: Atmospheres*, 114, 2009.
- 459 Ananthkrishnan, R. and Soman, M.: The onset of the southwest monsoon over Kerala: 1901–1980, *International Journal of Climatology*, 8,
460 283–296, 1988.
- 461 Ao, C. O., Waliser, D. E., Chan, S. K., Li, J.-L., Tian, B., Xie, F., and Mannucci, A. J.: Planetary boundary layer heights from GPS radio
462 occultation refractivity and humidity profiles, *Journal of Geophysical Research: Atmospheres*, 117, 2012.
- 463 Balaji, B., Prabha, T. V., Rao, Y. J., Kiran, T., Dinesh, G., Chakravarty, K., Sonbawne, S., and Rajeevan, M.: Potential of collocated radiometer
464 and wind profiler observations for monsoon studies, *Atmospheric Research*, 194, 17–26, 2017.
- 465 Bhat, G.: Near surface atmospheric characteristics over the North Bay of Bengal during the Indian summer monsoon, *Geophysical research
466 letters*, 28, 987–990, 2001.
- 467 Brown, A., Cederwall, R., Chlond, A., Duynkerke, P., Golaz, J.-C., Khairoutdinov, M., Lewellen, D., Lock, A., MacVean, M., Moeng, C.-H.,
468 et al.: Large-eddy simulation of the diurnal cycle of shallow cumulus convection over land, *Quarterly Journal of the Royal Meteorological
469 Society*, 128, 1075–1093, 2002.
- 470 Dethof, A., O'Neill, A., Slingo, J., and Smit, H.: A mechanism for moistening the lower stratosphere involving the Asian summer monsoon,
471 *Quarterly Journal of the Royal Meteorological Society*, 125, 1079–1106, 1999.
- 472 Ek, M. and Mahrt, L.: Daytime evolution of relative humidity at the boundary layer top, *Monthly Weather Review*, 122, 2709–2721, 1994.
- 473 Gadgil, S.: The Indian monsoon and its variability, *Annual Review of Earth and Planetary Sciences*, 31, 429–467, 2003.
- 474 Gadgil, S., Joseph, P., and Joshi, N.: Ocean–atmosphere coupling over monsoon regions, *Nature*, 312, 141–143, 1984.
- 475 Goswami, B. and Mohan, R. A.: Intraseasonal oscillations and interannual variability of the Indian summer monsoon, *Journal of Climate*,
476 14, 1180–1198, 2001.
- 477 Grabowski, W., Bechtold, P., Cheng, A., Forbes, R., Halliwell, C., Khairoutdinov, M., Lang, S., Nasuno, T., Petch, J., Tao, W.-K., et al.:
478 Daytime convective development over land: A model intercomparison based on LBA observations, *Quarterly Journal of the Royal Mete-
479 orological Society*, 132, 317–344, 2006.
- 480 Grabowski, W. W.: A parameterization of cloud microphysics for long-term cloud-resolving modeling of tropical convection, *Atmospheric
481 research*, 52, 17–41, 1999.
- 482 Grabowski, W. W.: Untangling microphysical impacts on deep convection applying a novel modeling methodology, *Journal of the Atmo-
483 spheric Sciences*, 72, 2446–2464, 2015.
- 484 Grabowski, W. W. and Morrison, H.: Untangling Microphysical Impacts on Deep Convection Applying a Novel Modeling Methodology.
485 Part II: Double-Moment Microphysics, *Journal of the Atmospheric Sciences*, 73, 3749–3770, 2016.
- 486 Grabowski, W. W. and Morrison, H.: Modeling condensation in deep convection, *Journal of the Atmospheric Sciences*, 74, 2247–2267, 2017.
- 487 Hansen, Z. R. and Back, L. E.: Higher surface Bowen ratios ineffective at increasing updraft intensity, *Geophysical Research Letters*, 42,
488 2015.
- 489 Joseph, P. and Sijkumar, S.: Intraseasonal variability of the low-level jet stream of the Asian summer monsoon, *Journal of Climate*, 17,
490 1449–1458, 2004.
- 491 Khairoutdinov, M. and Randall, D.: High-resolution simulation of shallow-to-deep convection transition over land, *Journal of the atmospheric
492 sciences*, 63, 3421–3436, 2006.



- 493 Kulkarni, J., Maheskumar, R., Morwal, S., Padmakumari, B., Konwar, M., Deshpande, C., Joshi, R., Bhalwankar, R., Pandithurai, G., Safai,
494 P., et al.: The cloud aerosol interactions and precipitation enhancement experiment (CAIPEEX): overview and preliminary results, *Curr.*
495 *Sci*, 102, 413–425, 2012.
- 496 Kusuma, G. R., Raman, S., and Prabhu, A.: Boundary-layer heights over the monsoon trough region during active and break phases,
497 *Boundary-Layer Meteorology*, 57, 129–138, 1991.
- 498 Lau, K. and Yang, S.: Seasonal variation, abrupt transition, and intraseasonal variability associated with the Asian summer monsoon in the
499 GLA GCM, *Journal of Climate*, 9, 965–985, 1996.
- 500 Murugavel, P., Malap, N., Balaji, B., Mehajan, R., and Prabha, T.: Precipitable water as a predictor of LCL height, *Theoretical and Applied*
501 *Climatology*, pp. 1–10, 2016.
- 502 Parasnis, S. and Goyal, S.: Thermodynamic features of the atmospheric boundary layer during the summer monsoon, *Atmospheric Environ-*
503 *ment. Part A. General Topics*, 24, 743–752, 1990.
- 504 Parasnis, S., Selvam, A. M., and Murty, B. V. R.: Variations of thermodynamical parameters in the atmospheric boundary layer over the
505 Deccan plateau region, India, *pure and applied geophysics*, 123, 305–313, 1985.
- 506 Prabha, T. V.: Cloud-Aerosol Interaction and Precipitation Enhancement experiment- recent findings, *Vayumandal*, pp. 1–18, http://imetsociety.org/wp-content/pdf/vayumandal/2014/2014_1.pdf, 2014.
- 508 Prabha, T. V., Khain, A., Maheshkumar, R., Pandithurai, G., Kulkarni, J., Konwar, M., and Goswami, B.: Microphysics of premonsoon and
509 monsoon clouds as seen from in situ measurements during the Cloud Aerosol Interaction and Precipitation Enhancement Experiment
510 (CAIPEEX), *Journal of the Atmospheric Sciences*, 68, 1882–1901, 2011.
- 511 Rajeevan, M., Gadgil, S., and Bhate, J.: Active and break spells of the Indian summer monsoon, *Journal of earth system science*, 119,
512 229–247, 2010.
- 513 Resmi, E., Malap, N., Kulkarni, G., Murugavel, P., Nair, S., Burger, R., and Prabha, T. V.: Diurnal cycle of convection during the CAIPEEX
514 2011 experiment, *Theoretical and applied climatology*, 126, 351–367, 2016.
- 515 Sakradzija, M. and Hohenegger, C.: What determines the distribution of shallow convective mass flux through cloud base?, *Journal of the*
516 *Atmospheric Sciences*, 2017.
- 517 Sandeep, A., Rao, T. N., Ramkiran, C., and Rao, S.: Differences in atmospheric boundary-layer characteristics between wet and dry episodes
518 of the Indian summer monsoon, *Boundary-layer meteorology*, 153, 217–236, 2014.
- 519 Sathyanadh, A., Karipot, A., Ranalkar, M., and Prabhakaran, T.: Evaluation of soil moisture data products over Indian region and analysis of
520 spatio-temporal characteristics with respect to monsoon rainfall, *Journal of Hydrology*, 542, 47–62, 2016.
- 521 Shutts, G. and Gray, M.: Numerical simulations of convective equilibrium under prescribed forcing, *Quarterly Journal of the Royal Meteoro-*
522 *logical Society*, 125, 2767–2787, 1999.
- 523 Skamarock, W. C., Klemp, J. B., Dudhia, J., Gill, D. O., Barker, D. M., Wang, W., and Powers, J. G.: A description of the advanced research
524 WRF version 2, Tech. rep., National Center For Atmospheric Research Boulder Co Mesoscale and Microscale Meteorology Div, 2005.
- 525 Stevens, B.: On the growth of layers of nonprecipitating cumulus convection, *Journal of the atmospheric sciences*, 64, 2916–2931, 2007.
- 526 Tompkins, A. M.: Organization of tropical convection in low vertical wind shears: The role of cold pools, *Journal of the atmospheric sciences*,
527 58, 1650–1672, 2001.
- 528 Yin, M. T.: Synoptic-aerologic study of the onset of the summer monsoon over India and Burma, *Journal of Meteorology*, 6, 393–400, 1949.